REGULAR ARTICLE

blood advances

Hapln1b, a central organizer of the ECM, modulates kit signaling to control developmental hematopoiesis in zebrafish

Christopher B. Mahony,[1,2] Pietro Cacialli,[1] Corentin Pasche,[1] Rui Monteiro,[2] Savvas N. Savvides,[3] and Julien Y. Bertrand[1]

[1]Department of Pathology and Immunology, Faculty of Medicine, University of Geneva, Geneva, Switzerland; [2]Institute of Cancer and Genomic Sciences, College of Medical and Dental Sciences, University of Birmingham, United Kingdom; and [3]Department of Biochemistry and Microbiology, VIB (Vlaams Instituut voor Biotechnologie)-UGent Center for Inflammation Research, Ghent, Belgium

Key Points

- *Hapln1b* encodes a structural protein that is absolutely necessary for hematopoietic stem cell emergence.
- The ECM is necessary for vasculature development, but also for kit signaling in the major vessels, to promote definitive hematopoiesis.

During early vertebrate development, hematopoietic stem and progenitor cells (HSPCs) are produced in hemogenic endothelium located in the dorsal aorta, before they migrate to a transient niche where they expand to the fetal liver and the caudal hematopoietic tissue, in mammals and zebrafish, respectively. In zebrafish, previous studies have shown that the extracellular matrix (ECM) around the aorta must be degraded to enable HSPCs to leave the aortic floor and reach blood circulation. However, the role of the ECM components in HSPC specification has never been addressed. In this study, *hapln1b*, a key component of the ECM, was specifically expressed in hematopoietic sites in the zebrafish embryo. Gain- and loss-of-function experiments all resulted in the absence of HSPCs in the early embryo, showing that *hapln1b* is necessary, at the correct level, to specify HSPCs in the hemogenic endothelium. Furthermore, the expression of *hapln1b* was necessary to maintain the integrity of the ECM through its link domain. By combining functional analyses and computer modeling, we showed that *kitlgb* interacts with the ECM to specify HSPCs. The findings show that the ECM is an integral component of the microenvironment and mediates the cytokine signaling that is necessary for HSPC specification.

Introduction

The emergence of blood cells is a highly conserved process that consists of many different waves in distinct anatomical locations. The first cells that emerge in zebrafish and mammals consist of primitive myeloid and erythroid cells,[1-4] Definitive hematopoiesis is then initiated by the emergence of the transient erythromyeloid precursors (EMPs), which arise in the yolk sac in mice and humans[1,2] and in the posterior blood island in zebrafish embryos.[5] Hematopoietic stem and progenitor cells (HSPCs) are then specified in the aorta-gonads-mesonephros (AGM) region, where they form small intra-aortic clusters.[6-11] HSPCs are derived directly from the aortic hemogenic endothelium (HE), and specification is controlled by the correct balance of several extrinsic factors, such as VEGF, hedgehog, notch, BMP, and transforming growth factor β signaling.[12-16] Early HSPC specification from the HE in zebrafish is marked by the expression of *gata2b*[17] followed by *runx1*.[12] Budding of zebrafish HSPCs occurs between 32 and 60 hours post fertilization (hpf), from the HE in the dorsal aorta.[18,19] This process is dependent on inflammatory cytokines produced by neutrophils and macrophages.[20-22] Macrophage- and vascular-mediated

Submitted 21 January 2020; accepted 30 June 2021; prepublished online on *Blood Advances* First Edition 20 September 2021; final version published online 30 November 2021. DOI 10.1182/bloodadvances.2020001524.

All important information can be obtained by contacting the corresponding authors (c.mahony@bham.ac.uk and julien.bertrand@unige.ch). All raw data will be accessible on the YARETA public server once the manuscript is accepted using this DOI: 10.26037/yareta:gkc7f4ro4rbnfioo7ryiqpwqda

The full-text version of this article contains a data supplement.

extracellular matrix (ECM) degradation is also necessary to enable HSPCs to migrate into the veins.[23,24] They then migrate to the caudal hematopoietic tissue (CHT), where they interact with endothelial cells and expand significantly in number.[25,26]

The exact mechanisms controlling HSPC emergence from the HE and their expansion in the CHT remain to be fully characterized. We and others have previously shown that these 2 processes are highly dependent on cytokine signaling. In particular, in zebrafish, we showed the important and nonredundant roles of oncostatin M and kit-ligand b (*kitlgb*) in this process.[25,27] Proteoglycans, major components of the ECM, interact with several hematopoietic cytokines (granulocyte-macrophage colony-stimulating factor, interleukin-3, and Kitlg) and maintain the proximity of stromal cells, HSPCs and cytokines in the niche.[28-30] We studied the role of *hapln1b*, an ECM-associated protein, in this process. We focused on *hapln1b*, as it has been shown to be expressed in the vasculature and hematopoietic tissues.[31] Furthermore, this gene is important for correct vascular development of the tail vasculature.[31] In mammals, there are *HAPLN1*, *2*, *3*, and *4* genes,[32] whereas in zebrafish, there are *hapln1a*, *1b*, *2*, *3*, and *4*.[31] *Hapln1* codes for a link protein, required to attach several chondroitin sulfate proteoglycans to the hyaluronic acid (HA) backbone (a ubiquitous glycosaminoglycan) to make large, negatively charged, ECM structures.[33] In mammals, *Hapln1* is a secreted ECM protein that stabilizes aggrecan-hyaluronan complexes and is required for correct craniofacial[34] and neocortex development.[35] Loss of *HAPLN1* expression promotes melanoma metastasis, but is also necessary to maintain immune cell motility.[36] *HAPLN1* is essential for maintaining lymphatic vessel integrity and reducing endothelial cell permeability, thus preventing visceral metastasis.[37] Knockout mouse studies have also revealed a role in maintaining perineural nets (PNNs), a hyaluronan backbone meshlike network of proteins that surround neurons and regulate neuronal plasticity,[38] as well as neural differentiation and development.[39-41] Furthermore, PNNs are responsible for binding chemorepulsive molecules, such as *Semaphorin3a*,[42] and transcription factors, such as *Otx2*, that are exchanged between different neural cells to enhance cortical plasticity.[43] *Hapln1a* was recently shown to be necessary for ECM expansion in the developing zebrafish heart, and CRISPR-Cas9 *hapln1a* mutants show reduced atrial size and chamber ballooning.[44] *Hapln1a* is also necessary for maintaining HA stability, therefore stabilizing the ECM,[45] and *sema3d*, for mediating signal transduction in skeletal growth and patterning in fin regeneration.[46]

In this study, *hapln1b* was necessary for mediating *kitlgb-kitb* interactions and inducing *runx1* expression in the HE during HSPC specification in the zebrafish embryo. Gain and loss of function of *hapln1b* both resulted in defective hematopoiesis. Therefore, we conclude that this gene is essential, at the correct dosage, for the specification of HSPCs from the HE and their development after their emergence.

Materials and methods

Zebrafish strains and husbandry

AB* (WT) zebrafish, along with transgenic and mutant strains were kept in a 14-/10-hour light/dark cycle at 28°C.[47] We used the following transgenic animals: *lmo2:eGFP*^{zf71},[48] *gata1:DsRed*^{sd2},[49] *kdrl:eGFP*^{s843},[50] *kdrl:Hsa.HRAS-mCherry*^{s896},[51] *cmyb:GFP*^{zf169},[52] *globin:eGFP*^{cz332},[53] *sox10:mRFP*^{vu234},[54] *mpx:GFP*^{i113},[55] and *mpeg1:mcherry*^{gl23}.[56] All animals were zebrafish embryos aged less than 120 hours post fertilization (hpf); therefore, there was no requirement for authorization of animal experimentation. However, our adult animals were raised according to the animal facilities guidelines of the University of Geneva.

WISH staining and analysis

Whole mount in situ hybridization (WISH) was performed on 4% paraformaldehyde-fixed embryos at the developmental time points indicated. Digoxygenin-labeled probes were synthesized with an RNA Labeling kit (SP6/T7; Roche). RNA probes were generated by linearization of TOPO-TA or ZeroBlunt vectors (Invitrogen) containing the polymerase chain reaction–amplified complementary DNA sequence. WISH was performed as previously described.[57] Phenotypes were scored by comparing expression with siblings. All injections were repeated 3 independent times. Analysis was performed with R or GraphPad Prism software. Embryos were imaged in 100% glycerol with an Olympus MVX10 microscope. The oligonucleotide primers used for the production of ISH probes are listed in supplemental Table 2.

Western blot analysis

Pools of ~30 embryos were collected. Cells were lysed in IP Lysis Buffer (IP Lysis Buffer) with protease inhibitor cocktail (Merck), and protein was extracted and then separated by gel electrophoresis and incubated overnight at 4°C with anti-HA antibody (1:1000 ab18181; abcam) followed by goat anti-mouse IgG (H+L)-horseradish peroxidase conjugate (1706516; BioRad). Staining was revealed by using Western Bright Sirius (1:1; Adventa) and an exposure of 1 minute, 15 seconds.

Cell sorting and flow cytometry

Zebrafish transgenic embryos (15-20 per biological replicate) were incubated in 0.5 mg/mL Liberase (Roche) solution and shaken for 90 minutes at 33°C, then dissociated, filtered, and resuspended in 0.9× phosphate-buffered saline and 1% fetal calf serum. Dead cells were labeled and excluded by staining with 5 nM Sytox red (Life Technologies) or 300 nM DRAQ7 (Biostatus). Cell sorting was performed on the Aria II (BD Biosciences) or the nS3 (BioRad). Data were analyzed with FlowJo and GraphPad Prism.

Quantitative real-time PCR and analysis

RNA was extracted with the Qiagen RNeasy minikit (Qiagen) and reverse transcribed into cDNA with a Superscript III kit (Invitrogen) or qScript (Quanta Biosciences). Quantitative PCR (qPCR) was performed with the Sybr Fast Universal qPCR kit (Kapa Biosystems) and run on the CFX Connect real-time system (BioRad). All primers are listed in supplemental Table 1. Analyses were performed with Microsoft Excel or GraphPad Prism.

Synthesis of full-length mRNA and microinjection

The PCR primers used to amplify the cDNA of interest are listed in supplemental Table 2. *Kitlgb* and *kitlga* messenger RNA (mRNA) was synthesized and injected as previously described.[25,27] mRNA was reverse transcribed with the mMessage mMachine kit SP6 (Ambion) from a linearized pCS2^{+} vector containing PCR products. After transcription, RNA was purified by phenol chloroform extraction. *Hapln1b* mRNA was injected at 200 pg, unless otherwise stated.

Immunofluorescence

Images were obtained with a Nikon SMZ1500 microscope or a Nikon inverted A1r spectral confocal microscope. Confocal z-stack image acquisition in multiple fluorescent channels was used to examine the entire dorsal aorta in the AGM . Immunofluorescence double staining was performed as described previously,[58] with anti-*p*-akt S473 (1:25; cat. no. 9271; Cell Signaling) and AlexaFluor 594–conjugated anti-rabbit secondary antibody (1:1000; cat. no. A11012; Life Technologies).

Imaging

WISH products were imaged on an Olympus MVX10 microscope in 100% glycerol. Fluorescent images were taken with an IX83 microscope and processed by CellSens Dimension software (Olympus). All images were processed with Adobe Photoshop. Time-lapse imaging was obtained with a Nikon inverted A1r spectral confocal microscope, processed with Fiji, and analyzed with GraphPad Prism.

Morpholinos

All morpholino oligonucleotides (MOs) were purchased from Gene Tools and are listed in supplemental Table 3. MO efficiency was tested by using PCR from total RNA extracted from a pool of 8 to 10 embryos at 24 hpf. *Hapln1b* full-length primers (supplemental Table 2) were used to test MO efficiency. The *hapln1b* morpholino was injected at 3 ng, unless otherwise stated. All MOs used were splice-blocking MOs.

Structural modeling and electrostatic properties of *kitlga* and *kitlgb*

Structural models for zebrafish kitlga and kitlgb were constructed based on a consensus approach using homology-modeling, template-based structure modeling, and ab initio structure prediction as implemented in i-TASSER, Phyre2, and RaptorX.[59-61] Vacuum electrostatic potential calculations were performed and displayed with the built-in module in PyMOL v. 2.3 (https://pymol.org/2/). Isoelectric point calculations were performed via the Prot-pI server (https://www.protpi.ch).

Results

Hapln1b is specifically expressed in early embryonic hematopoietic tissues

Previous studies have shown that *hapln1b* is expressed in the vasculature at 24 to 28 hpf, and that its loss of function results in abnormal angiogenesis.[31] However, its role during embryonic hematopoiesis has never been investigated. In zebrafish, *hapln1b* is the only *hapln* family member to display a hematopoietic expression pattern (Figure 1; supplemental Figure 1A), despite retaining high sequence identity and conserved peptides capable of forming disulphide bonds (supplemental Figure 1A-B). Synteny, phylogeny, and sequence identity analyses revealed that *hapln1a* and *hapln1b* originate from a duplication of the *HAPLN1* gene in mammals (supplemental Figure 2A-B). Even across these species, peptides capable of forming disulphide bonds within the link domain have been conserved (supplemental Figure 2C). We therefore focused our study on *hapln1b* and first examined its expression pattern. We established that *hapln1b* is initially expressed at ~12 hpf and would therefore not be derived from maternal RNA[62] (supplemental Figure 4A). *Hapln1b* is expressed between 20 and 26 hpf along the aorta, in the developing CHT and in the hypochord, as previously described.[31] Further analyses at 26 hpf revealed that *hapln1b* is also expressed in the aorta and vein region, ventral to the notochord (Figure 1Ai). The expression may be within the DA/PCV joint.[63] Between 30 and 36 hpf the expression begins to decrease, becoming more localized to the CHT, before being completely restricted to the marginal fold at 48 hpf (Figure 1A). Expression was also scored in the cardiac precursors at 36 hpf and in possible cranial cartilaginous structures (Figure 1Aii-iii). By 4 and 5 days post fertilization (dpf) expression was restricted to the cranial structures and was absent from the hematopoietic tissue (Figure 1B).

We then further analyzed the expression of *hapln1b* in different cell populations. We sorted endothelial cells from dissected *kdrl:eGFP* embryos at 26 and 48 hpf (Figure 1C), as previously described.[25] Consistent with the WISH, *hapln1b* was enriched in endothelial cells extracted from whole embryos at 26 hpf (Figure 1D) but no enrichment was noted at 48 hpf (Figure 1E), concordant with our WISH data. However, *hapln1b* was also highly enriched in early EMPs (*lmo2:GFP*$^+$ *gata1:DsRed*$^+$ cells at 28 hpf)[5] and nascent HSPCs (*kdrl:mCherry*$^+$ *cmyb:GFP*$^+$ cells at 36 hpf),[18] compared with whole embryos at 28 hpf (Figure 1F), which showed a potential link between *hapln1b* and embryonic definitive hematopoiesis. Amino acid structural analysis (using SMART; http://smart.embl.de/) revealed that *hapln1b* contains an immunoglobulin domain and 2 HA link domains (Figure 1G). We next investigated how this ECM protein interferes with developmental hematopoiesis.

Hapln1b is necessary for specifying HSPCs from the HE

To further investigate the role of this gene in hematopoiesis, we injected a splice-blocking MO for *hapln1b*. This process efficiently reduced the mRNA levels (supplemental Figure 4B-C), either because the nonspliced RNA was too long to be amplified, or because the resulting RNA was degraded. Inhibiting *hapln1b* expression did not affect *gata2b* expression, the earliest known marker of HE specification[17] (Figure 2A). However, *runx1* and *cmyb* expression was robustly decreased in the aortic region (Figure 2A). Accordingly, additional downstream expression of *cmyb* at 4 dpf in the CHT and *rag1* at 4.5 dpf in the thymus were also decreased (Figure 2A-C). To further validate the specificity of our MO, we then rescued the loss of *runx1* in *hapln1b* morphants by coinjecting the MO with *hapln1b* mRNA (supplemental Figure 4D). *Hapln1b* morphants displayed normal vascular specification, although in some cases the formation of the CHT was perturbed, as seen in the "mild" cases (Figure 2D) and as previously described.[31] In a small number of embryos, the vasculature was severely affected as represented in the "severe" phenotype (Figure 2D). We then further analyzed the development of both the aorta and vein and found that *hapln1b* morphants had an increased diameter of the vein and a slight decreased aortic diameter (supplemental Figure 3A-B). We observed no change in the emergence of primitive macrophages or red blood cells, as marked by *mfap4* and *gata1* at 24 hpf (Figure 2E), respectively, although some embryos displayed a decrease in *mfap4* cells in the tail region, possibly because of disrupted vasculature formation (Figure 2E). We noted, however, a decrease in primitive circulating neutrophils, as marked by *mpx* (Figure 2E), although neutrophils were still present on the yolk sac. This change in

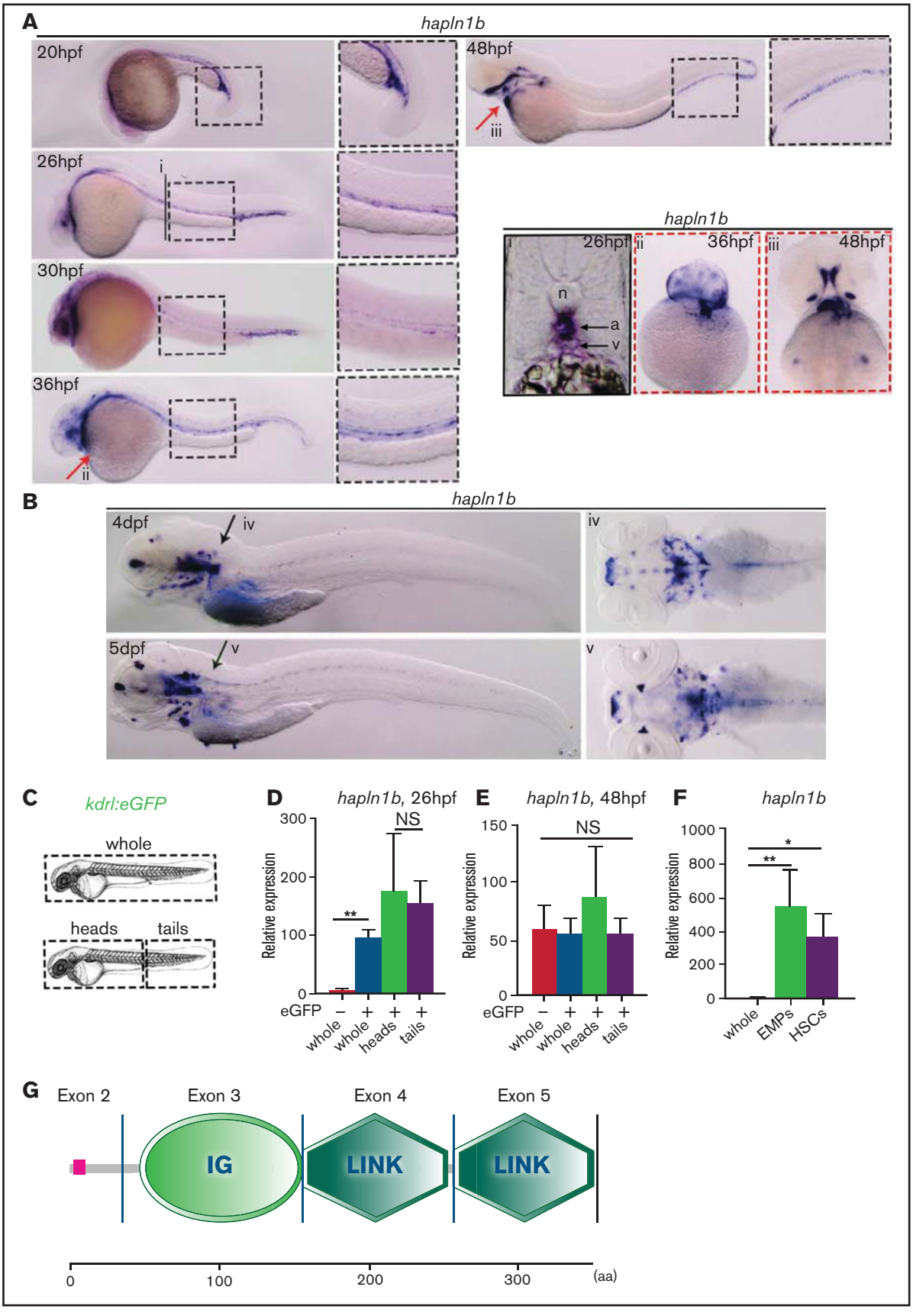

Figure 1. *Hapln1b* is expressed by vascular cells and hematopoietic progenitors. (A) WISH of *hapln1b* expression from 20 to 48 hpf. (Ai) Section at 26 hpf, displaying aorta (a) and vein (v) and notochord (n). (Aii-iii) ventral view at 36 and 48 hpf. (B) WISH of *hapln1b* expression at 4 and 5 dpf. (Biv-v) Dorsal view at 4 and 5 dpf.

distribution, as for macrophages, may be related to the loss of function of the vasculature depicted in Figure 2D. Loss of *hapln1b* thus results in a loss of HSPCs but does not affect primitive hematopoiesis. We next sought to confirm the loss of HSPCs in *hapln1b* morphants by using confocal imaging in double-transgenic *kdrl:mCherry;cmyb:eGFP* embryos. The images revealed a similar decrease in HSPC budding (Figure 2F) that correlated with the loss of *runx1* and *cmyb* expression shown in Figure 2A, but no change in circulating cells when imaged at 30 hpf (supplemental Movies 1 [control (ctrl) MO; n = 3] and 2 [h1b MO; n = 3]). We then investigated the effect of *hapln1b* overexpression on embryonic hematopoiesis.

Hapln1b overexpression is sufficient to reduce HSPC emergence and downstream survival

We next induced overexpression of *hapln1b* by injecting the full-length mRNA at the 1-cell stage and analyzed the effect on developmental hematopoiesis. *Hapln1b* overexpression did not change HE programming, vessel development, and early HSPC specification, as marked by *gata2b* at 22 hpf, *kdrl* at 24 hpf, and *runx1* at 28 hpf, respectively (Figure 3A). However, on further investigation, we found that the aorta presented a smaller diameter, whereas the vein was unaffected (supplemental Figure 3C-D). Moreover, we noted a decrease in *cmyb* signal at 36 hpf in the AGM region (Figure 3A). *Hapln1b* overexpression also decreased *cmyb* signal at 48 hpf in the CHT, suggesting that newly formed HSPCs did not colonize this tissue. The absence of the *cmyb* signal along the aorta, as in the non-injected controls, indicated that HSPCs were not lodged and were not unable to migrate from the aorta (Figure 3B). Accordingly, *rag1* staining in the thymus at 4.5 dpf and *cmyb* in the CHT at 4 dpf were also decreased (Figure 3C). To further analyze this loss of *cmyb* signal, we then imaged double-positive *kdrl*:mCherry;*cmyb*:eGFP embryos to examine HSPC emergence from the HE.[18] *Hapln1b* overexpression significantly reduced the number of double-positive, nascent HSPCs in the AGM region at 36 and 48 hpf (Figure 3D-D′). As expected, the number of HSPCs present in the CHT niche at 3 and 4 dpf was also significantly reduced (Figure 3E- E′). To further examine this loss of *cmyb* at 36 hpf from the HE, we used time-lapse confocal microscopy to image double-positive *kdrl*:mCherry;*cmyb*:eGFP embryos and examine the endothelial-to-hematopoietic transition events in the aorta. We imaged from 34 to 42 hpf to observe HSPC budding from the HE. We observed clusters of cells in the AGM region of control embryos, preparing to bud and enter circulation (supplemental Movies 3 and 4). However, in *hapln1b*-overexpressing embryos, almost no cells initiated budding. Occasionally, some *cmyb:GFP*$^{+}$ cells were detected, but none underwent endothelial-to-hematopoietic transition (supplemental Movies 5 and 6). We then examined blood circulation at 28 hpf after mRNA injection and found normal circulation in 6 of 10 control (non-injected) embryos (supplemental Movie 7). Only 4 of 10 *hapln1b*-overexpressing embryos (supplemental Movie 8) showed normal circulation, whereas 6 of 10 embryos showed slower blood circulation. We therefore concluded that *hapln1b* overexpression is sufficient to prevent normal HSPC budding from the HE.

We next investigated how *hapln1b* affects cytokine signaling in the aortic region, which could be responsible for controlling HSPC differentiation.

Hapln1b mediates the *kitlgb-kitb* interactions that are necessary for proper HSPC specification from the HE

We next attempted to decipher the mechanism by which *hapln1b* affects hematopoiesis. Our previous studies indicated that HSPCs express *kitb* and that *kiltgb* and *kitb* are essential for *runx1* expression in the HE at 28 hpf.[27] As we found a similar decrease in *runx1* in *hapln1b* morphants, we investigated a possible link between *kiltgb* signaling and *hapln1b*. Previous studies have indicated that *kitlgb* is expressed in the CHT region by ISH at 24 hpf and is likely to exist more commonly as the membrane-bound form, because of a loss of 1 of the 2 cleavage sites.[64] By contrast, *kitlga* represents the more soluble form of this ligand, as it retains the 2 cleavage sites.[64] We also investigated the expression of *kiltgb* in fluorescence-activated cell sorting (FACS)–sorted cells and found no enrichment in *globin*:GFP^{+} cells at 20 hpf, primitive macrophages sorted from *mpeg1*:mcherry embryos at 24 hpf, primitive neutrophils sorted from *mpx*:eGFP embryos at 24 hpf, or neural crest cells sorted from *sox10*:mRFP embryos at 26 hpf (supplemental Figure 5A-D). We also found no enrichment of *kitlgb* in endothelial cells sorted from dissected embryos at 19 to 20 hpf (supplemental Figure 5E). However, we found a significant enrichment in tail endothelial cells at 26 hpf (supplemental Figure 5F), consistent with the previously published ISH expression pattern of *kitlgb*.[64] We therefore concluded that *kiltgb* would be present in the AGM at low concentrations and that an additional element would be needed to mediate effective interaction with its receptor to initiate *runx1* expression. We tested this hypothesis by attempting to rescue the loss of *runx1* observed in *hapln1b* morphants and the loss of *cmyb* observed in *hapln1b*-overexpressing embryos by injecting *kitlgb* mRNA.

To verify the specificity of our *kitlgb* injection, we also injected *kitlga* mRNA, which does not play any role in HSPC specification and development.[27] Injection of either *kitlga* or *kitlgb* did not alter the expression of *runx1* at 28 hpf, as anticipated. Injection of the *hapln1b* MO induced a similar loss of *runx1* at 28 hpf (Figure 4A-A′). We then coinjected the *hapln1b* MO with *kitlgb* mRNA, which resulted in a rescue of the *runx1* signal in 16 of 34 embryos (Figure 4A-A′). As expected, *kiltga* did not rescue the loss of *runx1* in *hapln1b* morphants (Figure 4A-A′). We then attempted to rescue the decrease of *cmyb* signal in the *hapln1b*-overexpressing embryos by injecting *kitlgb* mRNA. Compared with non-injected controls, *hapln1b* mRNA reduced *cmyb* expression at 36 hpf, as

Figure 1. (continued) (C-E) Experimental outline and qPCR expression of *hapln1b* from FACS-sorted endothelial cells. (F) qPCR expression of *hapln1b* in FACS-sorted hematopoietic progenitors (EMPs and HSPCs). All qPCR data are from biological triplicates (except for whole GFP^{-} in panel D, where data represent biological duplicates). Data indicate expression relative to *ef1a* (calculated by [^{2}Ct(*hapln1b*) − Ct(*ef1a*)] × 10 000). (D) Two-tailed Student *t*-test, whole GFP^{-} and GFP^{+}; $P = .0035$; heads and tails, $P = .75$. (E-F) Analysis was performed by 1-way analysis of variance with multiple comparisons. (E) Whole GFP^{-} and GFP^{+}, $P = .99$; whole GFP^{-} and heads, $P = .44$; and whole GFP^{-} and tails, $P = .99$. (F) Whole and EMPs, $P = .0081$; whole and HSPCs, $P = .0449$. (G) SMART (http://smart.embl.de/) prediction of hapln1b protein structure. IG, immunoglobulinlike domain; Link, HA Link domain; aa, amino acid.

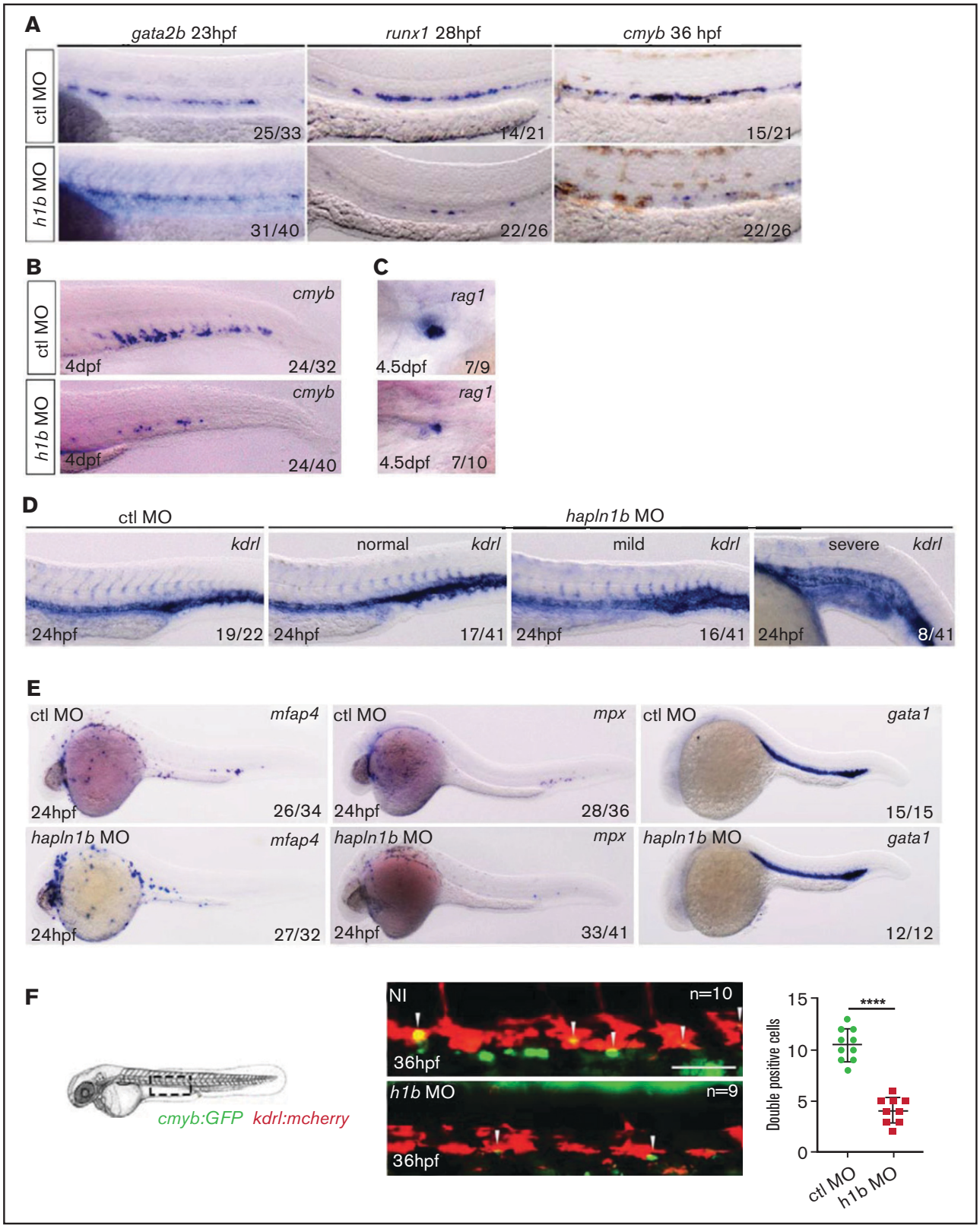

Figure 2. *Hapln1b* is necessary for the specification of HSPC from the hemogenic endothelium. (A) *Gata2b*, *runx1*, and *cmyb* ISH in control MO, or *hapln1b* MO-injected embryos (injected at 3 ng throughout, unless otherwise stated). (B) ISH expression of *cmyb*, in control MO–, or *hapln1b* MO–injected embryos. (C) *Rag1* expression in the thymus after control MO or *hapln1b* MO injection. (D) ISH expression of *kdrl* in control MO– or *hapln1b* MO–injected embryos. *Hapln1b* morphants displayed 3 phenotypes: normal, mild, and severe. (E) ISH expression of *mfap4*, *mpx*, and *gata1* in control MO– or *hapln1b* MO–injected embryos. H1b, *hapln1b*. (F) Imaging double-transgenic *kdrl:mCherry/cmyb:GFP* embryos at 36 hpf. Bar represents 50 μm. Control (ctl) MO vs *hapln1b mRNA* injected, $P < .0001$. Student unpaired *t*-test.

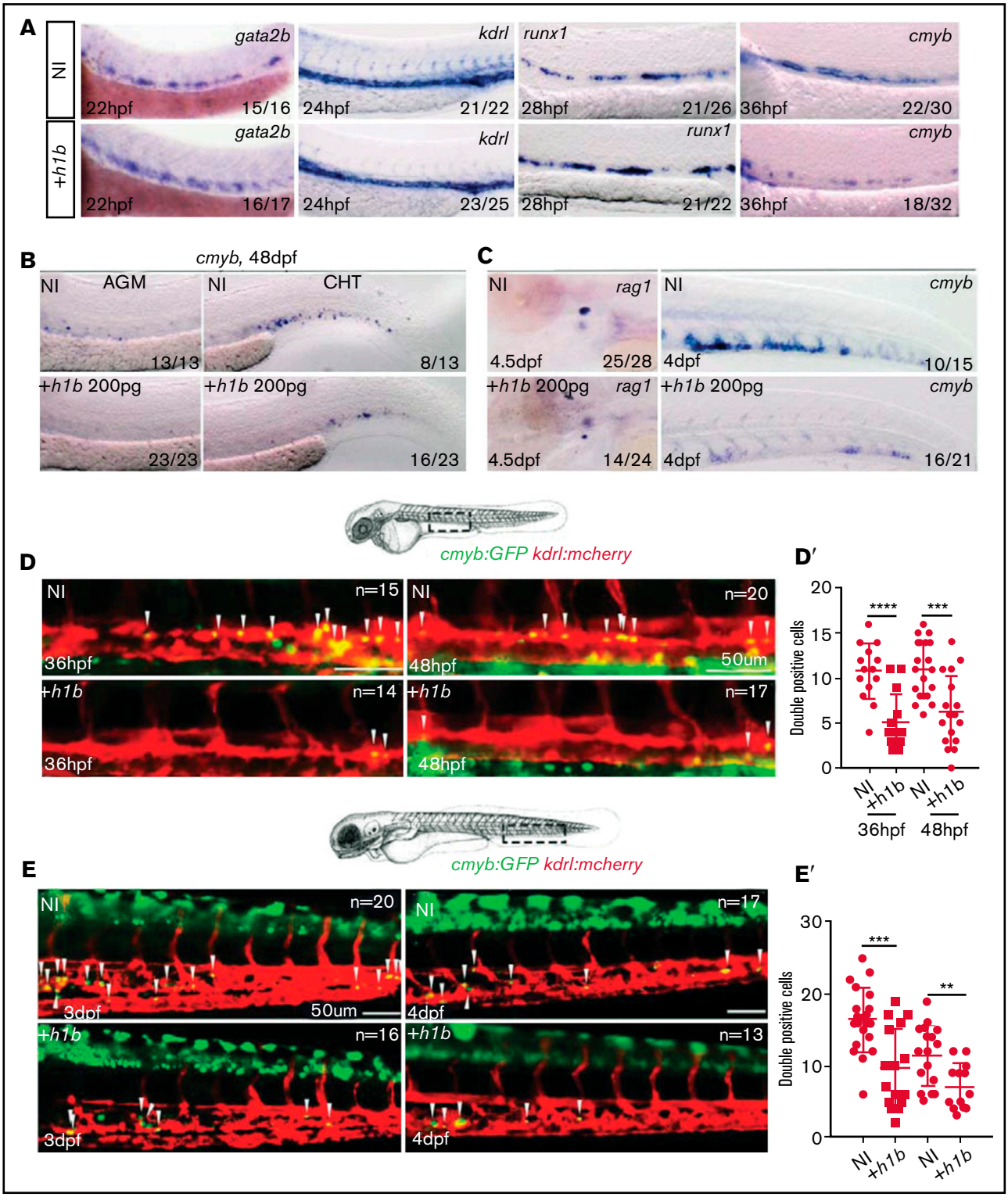

Figure 3. *Hapln1b* overexpression inhibits HSPC budding and development. (A) ISH expression of *kdrl*, *runx1*, and *cmyb* in non-injected or *hapln1b* mRNA–injected embryos. (B-C) ISH expression of *cmyb* in non-injected or *hapln1b* mRNA–injected embryos. (D-D′) Double-transgenic *kdrl:mCherry/cmyb:GFP* embryos at 36 and 48 hpf. Bar represents 50 μm. (D′) NI vs +*h1b*-injected at 36 hpf, $P < .0001$; and at 48 hpf, $P = .0003$. (E-E′) Imaging double-transgenic *kdrl:mCherry/cmyb:GFP* embryos at 3 and 4 dpf. Bar represents 50 μm. (E′) NI vs +*h1b* injected at 3 dpf, $P = .0003$; and at 4 dpf, $P = .004$. NI, non-injected, +*h1b: hapln1b* mRNA–injected.

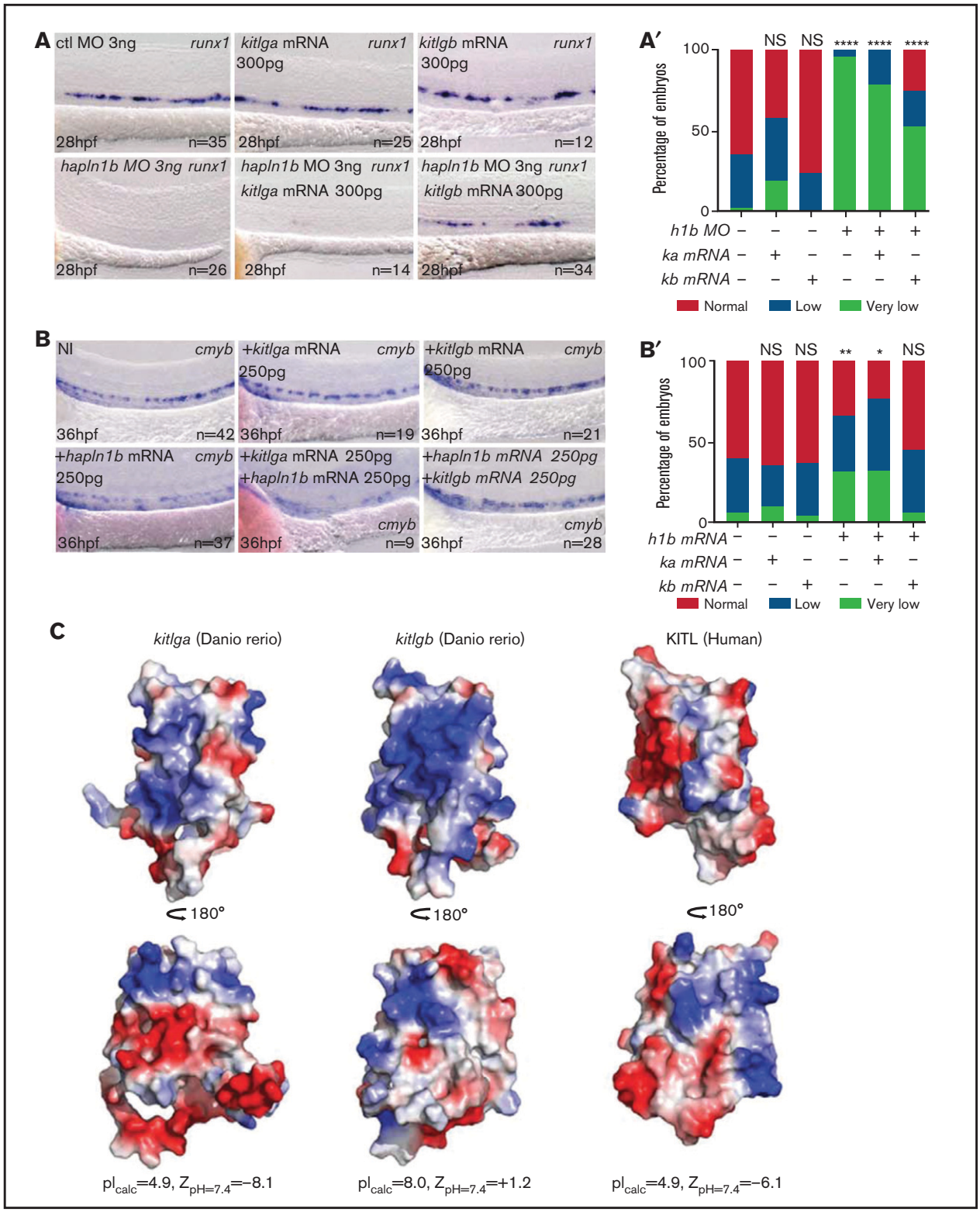

Figure 4. *Hapln1b* interacts with kitlgb to maintain kitlgb-kitb interactions in the AGM. (A) ISH expression pattern of *runx1* in control morphants, *kitlga* mRNA–injected embryos, *kitlgb* mRNA–injected embryos, *hapln1b* morphants, embryos injected with both *hapln1b* MO and *kitlga* mRNA, and embryos injected with both hapln1b MO and *kitlgb* mRNA. (A′) Analysis of *runx1* expression. All results are compared with control MO. Data were analyzed by Fisher's exact test using R. Control (ctl) MO vs +*kitlga*, $P = .05826$; NI vs +*kitlgb*, $P = .7939$; NI vs +*hapln1b*, $P < .0001$; NI vs +*hapln1b*+*kitlga*, $P < .0001$; and NI vs +*hapln1b*+*kitgb*: $P < .0001$. (B) ISH expression of *cmyb* in NI control embryos, *hapln1b* mRNA–injected embryos, *kitlgb* mRNA–injected embryos, and embryos injected with both *hapln1b* and *kitlgb*. (B′) analysis of *cmyb* expression. All analysis is compared with the NI control. Data were analyzed by Fisher's exact test using R. NI vs +*kitlga*, $P = .8373$; NI vs +*kitlgb*, $P = .99$; NI vs +*hapln1b*, $P = .0051$; NI vs +*hapln1b*+*kitlga*, $P = .036$; and NI vs +*hapln1b*+*kitgb*, $P = .8617$. h1b, hapln1b; ka, kitlga; Kb, kitlgb. (C) Electrostatic potential of *KITL*, *kiltga* and *kitlgb* at biological pH. Blue, positive charge; white, neutral charge; red, negative charge. NI, non-injected.

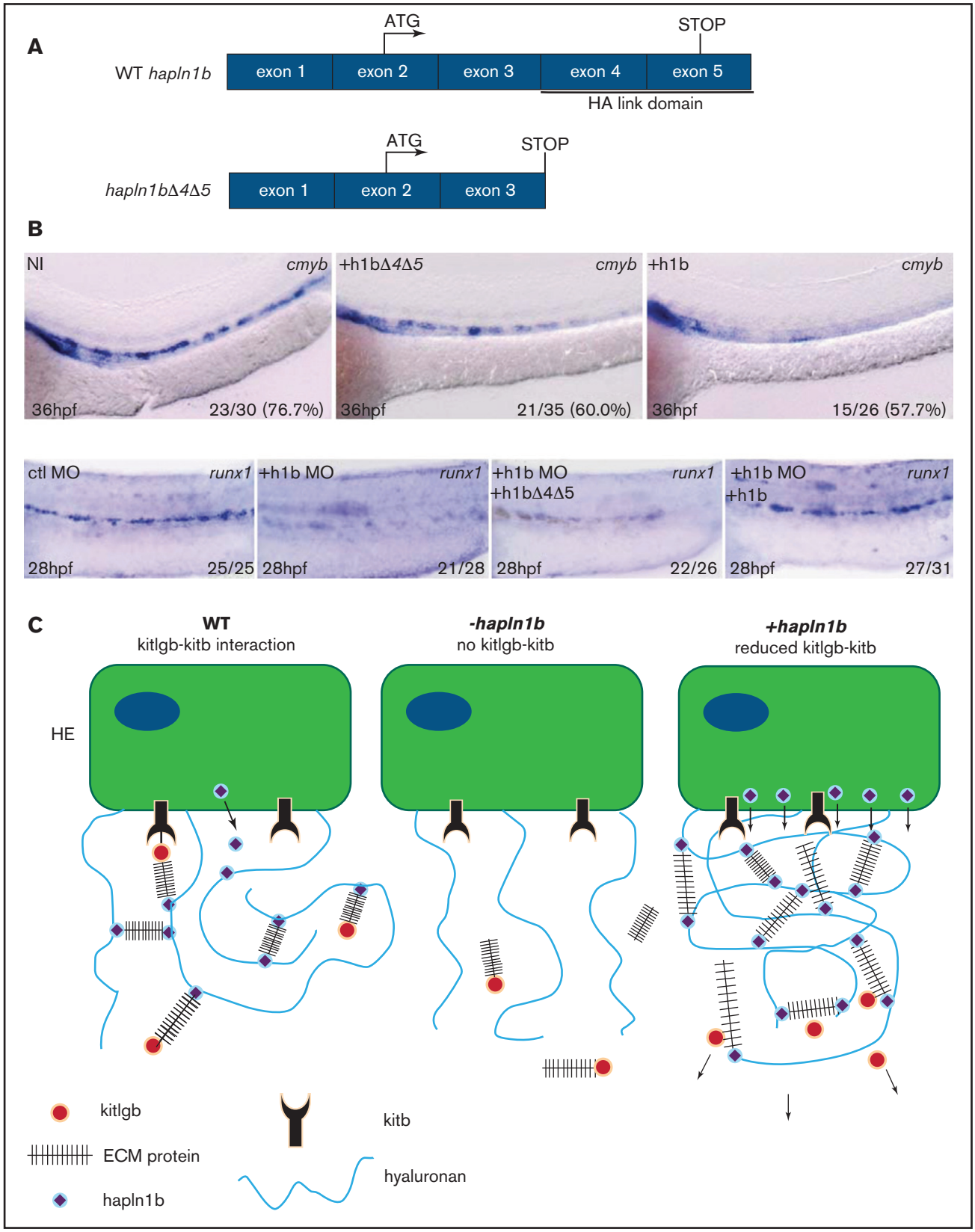

Figure 5. *Hapln1b* overexpression inhibits *cmyb* through interactions mediated by the link domains. (A) Schematic representation of WT *hapln1b* and a truncated version that lacks exons 4 and 5 (*hapln1b*Δ4Δ5). (B) ISH expression of *cmyb* in NI control embryos, *hapln1b* mRNA–injected embryos and *hapln1b*Δ4Δ5-injected embryos at 36 hpf. ISH expression of *runx1* in control MO (ctl MO), *hapln1b* MO (h1b MO), *hapl1b* MO, and *hapln1b*Δ4Δ5 mRNA–injected (h1b MO and h1bΔ4Δ5), and

observed earlier (Figure 4B-B′). Although *kitlgb* injection alone did not alter *cmyb* expression at 36 hpf (Figure 4B-B′), coinjection of both *hapln1b* and *kitlgb* mRNAs increased *cmyb* expression to control levels (Figure 4B-B′). Altogether, the data suggest that the dose of *hapln1b* controls accessibility of *kitlgb* to the HE.

As proteoglycans are negatively charged, we sought to examine the possible electrostatic compatibility of *kitlgb* with such a biological environment. In the absence of an experimentally determined structure for zebrafish *kitlgb* and *kitlga*, we leveraged available structural information at high resolution on human KITL (SCF) [65,66] and the related hematopoietic cytokines Flt3 ligand and colony-stimulating factor 1,[67-69] to derive reliable models based on homology-based approaches and ab initio structure prediction.

Our analysis revealed that *Kitlgb* would be expected to display an overall positive electrostatic potential as manifested by a Z-potential value of +1.2 mV at physiological pH and as illustrated by extensive patches of positively charged amino acids at the protein surface (Figure 4C). Such physicochemical properties are in sharp contrast to zebrafish *Kitlga* and human *KITL*, which are pronouncedly acidic with very similar electrostatic properties characterized by strongly negative electrostatic ζ-potentials at physiological pH. As proteoglycans are negatively charged, the overall positively charged *Kitlgb*, but not the negatively charged *Kitlga*, would mediate favorable interactions with the ECM in hemogenic and hematopoietic tissues, therefore activating the *Kitb* receptor, consistent with our findings.

Finally, to further confirm that *hapln1b* expression is necessary for *kitlgb* signaling we examined phospho-AKT, a downstream marker of the kit receptor activation.[70] Control MO– and *kitlgb* mRNA-injected embryos showed a robust increase in the number of phospho-AKT^{+} cells in the dorsal aorta (supplemental Figure 6A-B). *Hapln1b* morphants displayed a large decrease in phospho-AKT^{+} cells in the DA, which was rescued in *kitlgb* mRNA–injected *hapln1b* morphants (supplemental Figure 6A-B). We then coinjecting MOs at half doses and confirmed that signaling of both *hapln1b* and *kitlgb* is required for HSPC specification. Half-dose *hapln1b* morphants showed a moderate decrease in *runx1* (supplemental Figure 6C). Half-dose *kitlgb* morphants showed normal *runx1* expression (supplemental Figure 6C). Half-dose *hapln1b*/*kitlgb* double morphants showed a robust decrease in *runx1* expression (supplemental Figure 6C), suggesting an interaction of both genes to specify HSPCs.

The link domain is necessary for *hapln1b* functions

Finally, we wanted to verify that *hapln1b* interacts with HA through its link domain. We cloned a truncated version of the *hapln1b* mRNA lacking exons 4 and 5 (*hapln1b*Δ4Δ5), which encode the HA link domain (Figure 5A). Compared with the non-injected controls, *hapln1b*Δ4Δ5 mRNA–injected specimens did not show a reduction of *cmyb* levels at 36 hpf, whereas wild-type *hapln1b* mRNA–injected specimens did (Figure 5B), as shown earlier (Figure 3A). Furthermore, *hapln1b* full-length mRNA, and not *hapln1b*Δ4Δ5 mRNA, rescued the loss of *runx1* at 28 hpf, observed in *hapln1b* morphants (Figure 5B), when the product of both mRNAs (HA-tagged versions) were detected at 24 hpf (supplemental Figure 4E). We therefore concluded that the link domain is necessary for *hapln1b* to fulfill its function: the assembly of the ECM. We therefore propose the following model, wherein *kitlgb* is distributed along the aorta by interacting with the ECM. The ECM structure is maintained by proteoglycans forming links with the HA backbone (mediated by the link domain of *hapln1b*), enabling *kiltgb* to reach the AGM. A loss of *hapln1b* will prevent HA links from being formed and will prevent *kitlgb* distribution to the AGM, reducing *runx1* expression (Figure 5C). When *hapln1b* is overexpressed, HSPC budding is reduced as the HA links are increased, resulting in a tight ECM that would also reduce *kitlgb* distribution to the AGM. Therefore, a lower concentration of *kitlgb* in the AGM would result in the budding and development of fewer HSPCs (Figure 5C).

Discussion

We have shown that *hapln1b* is expressed along the embryonic endothelium before HSPC emergence, before it becomes restricted to non hematopoietic tissue at later stages (Figure 1). *Hapln1b* is required, in the correct concentration, to specify HSPCs from the HE and to maintain HSPC budding and release into circulation. We found that loss of *hapln1b* results in a loss of *runx1* and of downstream HSPC specification markers (Figure 2A-C). As proteoglycans can bind cytokines, it is possible that *hapln1b* is responsible for maintaining HA linking to proteoglycans to favor cytokine-receptor interaction. This notion was corroborated by a recent study showing that HA glycosaminoglycans are closely associated with early Flk1^{+} hematoendothelial cell progenitors during gastrulation and act as a cytokine trap to enhance VEGF-mediated angiogenesis and primitive hematopoiesis.[71] Our previous data have shown that *kitlgb-kitb* signaling is essential for maintaining *runx1* expression and HSPC specification in the HE.[27] However, we and others[64] have demonstrated that *kitlgb* is highly expressed in the posterior blood island but not in the aortic HE region. When we modulated *hapln1b* expression, we were able to change the structure of the ECM, as the loss of *hapln1b* affects the vasculature in the CHT vessels and affects the overall CHT structure (Figure 2D). The disruption of the CHT structure after *hapln1b* knockdown was also noted in a previous study.[31] This, coupled with the fact that *hapln1b* morphants were rescued with *kitlgb* mRNA injections (Figure 4A), leads us to conclude that *hapln1b* mediates HA linking with proteoglycans and is responsible for stabilizing the ECM scaffold and distributing *kitlgb* to the HE (Figure 5C). Our data show that the ECM most likely plays a crucial role in maintaining the signaling environment in proximity to the AGM, to mediate HSPC specification from the HE. Furthermore, our results showed an involvement of the ECM in the CHT, further suggesting that the ECM is a key player in maintaining the embryonic niche to help in expanding HSPCs. Although we have highlighted *kiltgb* as a key cytokine that interacts with the ECM, there are most likely many others that contribute to the extrinsic signaling microenvironment. Fully characterizing and

Figure 5. (continued) *hapl1b* MO and *hapln1b* full-length mRNA (h1bMO and h1b)–injected embryos at 28 hpf. (C) Summary of proposed model. In the wild-type situation, hapn1b helps *kitlgb* to interact with *kitb* in the AGM to permit runx1 expression and HSPC formation. Loss of *hapln1b* results in a loss of kitlgb interaction with kitb, no *runx1* expression, and no HSPCs forming. Overexpression of *hapln1b* results in a dense ECM and reduced kitlgb interaction with kitb, impairing HSPC emergence and survival. HE, hemogenic endothelium; NI, non-injected.

understanding these molecules is an important step in improving the currently challenging derivation of HSPCs from iPSCs.

In contrast to our loss-of-function assays, overexpression of *hapln1b* resulted in normal HSPC specification, as indicated by normal *runx1* expression (Figure 3A), but caused a reduction in HSPC emergence and later expansion within the hematopoietic tissue, as indicated by a reduction of *cmyb* expression (Figure 3B). As we found that HSPC emergence was reduced, but never completely ablated, we reasoned that overexpression of *hapln1b* is likely to result in a denser ECM, reducing the accessibility of *kitlgb* to the hemogenic microenvironment. We confirmed this by rescuing HSPC expansion in *hapln1b*-overexpressing embryos by overexpressing *kiltgb* mRNA (Figure 4B). Recent mouse studies have indicated that *Kitlg* is required throughout HSPC development in the AGM region.[72] This was further corroborated by additional studies showing that *c-kit* is expressed by proliferating HSPCs in the AGM[73] and that *Kitlg* maintains HSPCs in mouse AGM cultures.[74] It is therefore likely that reducing the concentration of *kitlgb* in our *hapln1b*-overexpressing embryos restricts HSPC emergence and decreases downstream survival and HSPC maturation (Figure 5C). It is also possible that the ECM is too dense to enable HSPC to bud and migrate to the CHT, as results in previous studies have indicated that ECM degradation, [23,24] biomechanical forces exerted by blood flow,[75] and mechanical instability in the aorta[76] are essential for HSPCs to enter the blood circulation.

A similar role for *Hapln1* has been demonstrated in the PNNs in the mouse central nervous system, as it is necessary for maintaining the HA mesh surrounding the neurons.[38] These PNNs bind molecules to maintain neuronal plasticity and development, further implicating this gene in maintaining the ECM. Recent studies have shown that HSPCs migrate to the fetal niche and the CHT and expand their initial number in response to several cytokines.[23,25,26] It is possible that many cytokine gradients and concentrations are maintained in the fetal niche by ECM components, such as *hapln1b*. Understanding them in more detail helps in fully characterizing HSPC expansion and provides alternative methods of improving HSPC expansion ex vivo.

Acknowledgments

J.Y.B. holds a Chair in Life Sciences funded by the Gabriella Giorgi-Cavaglieri Foundation and is also funded by the Swiss National Fund (310030_184814) and the "Fondation Privée des HUG". R.M. and C.B.M. were funded by a British Heart Foundation IBSR Fellowship (FS/13/50/30436).

Authorship

Contribution: S.N.S. performed structural analysis of *KITL*, *kitlga*, and *kitlgb*; C.B.M., P.C., and C.P. performed the experiments; C.B.M. and J.Y.B. designed the research and wrote the initial draft of the manuscript; and S.N.S. and R.M. edited the manuscript.

Conflict-of-interest disclosure: The authors declare no competing financial interests.

ORCID profiles: C.B.M., 0000-0003-4487-2540; P.C., 0000-0003-1250-0793; R.M., 0000-0002-4223-8506; J.Y.B., 0000-0001-6570-4082.

Correspondence: Christopher B. Mahony, Institute of Cancer and Genomic Sciences, University of Birmingham, Birmingham B152TT, United Kingdom; E-mail: c.mahony@bham.ac.uk; and Julien Y. Bertrand, University of Geneva, CMU, Rue Michel-Servet, 1, Geneva 4 1211, Switzerland; e-mail: julien.bertrand@unige.ch.

References

1. Bertrand JY, Jalil A, Klaine M, Jung S, Cumano A, Godin I. Three pathways to mature macrophages in the early mouse yolk sac. *Blood.* 2005;106 (9):3004-3011.
2. McGrath KE, Frame JM, Fegan KH, et al. Distinct Sources of Hematopoietic Progenitors Emerge before HSCs and Provide Functional Blood Cells in the Mammalian Embryo. *Cell Rep.* 2015;11(12):1892-1904.
3. Palis J. Primitive and definitive erythropoiesis in mammals. *Front Physiol.* 2014;5:3.
4. Palis J, Chan RJ, Koniski A, Patel R, Starr M, Yoder MC. Spatial and temporal emergence of high proliferative potential hematopoietic precursors during murine embryogenesis. *Proc Natl Acad Sci USA.* 2001;98(8):4528-4533.
5. Bertrand JY, Kim AD, Violette EP, Stachura DL, Cisson JL, Traver D. Definitive hematopoiesis initiates through a committed erythromyeloid progenitor in the zebrafish embryo. *Development.* 2007;134(23):4147-4156.
6. Boisset JC, van Cappellen W, Andrieu-Soler C, Galjart N, Dzierzak E, Robin C. In vivo imaging of haematopoietic cells emerging from the mouse aortic endothelium. *Nature.* 2010;464(7285):116-120.
7. Bollerot K, Pouget C, Jaffredo T. (2005a). The embryonic origins of hematopoietic stem cells: a tale of hemangioblast and hemogenic endothelium. *APMIS.* 2005;113: 790-803.
8. Bollerot K, Romero S, Dunon D, Jaffredo T. Core binding factor in the early avian embryo: cloning of Cbfbeta and combinatorial expression patterns with Runx1. *Gene Expr Patterns.* 2005b;6(1):29-39.
9. Chen MJ, Yokomizo T, Zeigler BM, Dzierzak E, Speck NA. Runx1 is required for the endothelial to haematopoietic cell transition but not thereafter. *Nature.* 2009;457(7231):887-891.
10. Jaffredo T, Gautier R, Brajeul V, Dieterlen-Lièvre F. Tracing the progeny of the aortic hemangioblast in the avian embryo. *Dev Biol.* 2000;224(2): 204-214.
11. Zovein AC, Hofmann JJ, Lynch M, et al. Fate tracing reveals the endothelial origin of hematopoietic stem cells. *Cell Stem Cell.* 2008;3(6):625-636.

12. Burns CE, Traver D, Mayhall E, Shepard JL, Zon LI. Hematopoietic stem cell fate is established by the Notch-Runx pathway. *Genes Dev.* 2005; 19(19):2331-2342.

13. Gering M, Patient R. Hedgehog signaling is required for adult blood stem cell formation in zebrafish embryos. *Dev Cell.* 2005;8(3):389-400.

14. Kim AD, Melick CH, Clements WK, et al. Discrete Notch signaling requirements in the specification of hematopoietic stem cells. *EMBO J.* 2014; 33(20):2363-2373.

15. Monteiro R, Pinheiro P, Joseph N, et al. Transforming Growth Factor β Drives Hemogenic Endothelium Programming and the Transition to Hematopoietic Stem Cells. *Dev Cell.* 2016;38(4):358-370.

16. Wilkinson RN, Pouget C, Gering M, et al. Hedgehog and Bmp polarize hematopoietic stem cell emergence in the zebrafish dorsal aorta. *Dev Cell.* 2009;16(6):909-916.

17. Butko E, Distel M, Pouget C, et al. Gata2b is a restricted early regulator of hemogenic endothelium in the zebrafish embryo. *Development.* 2015; 142(6):1050-1061.

18. Bertrand JY, Chi NC, Santoso B, Teng S, Stainier DY, Traver D. Haematopoietic stem cells derive directly from aortic endothelium during development. *Nature.* 2010;464(7285):108-111.

19. Kissa K, Herbomel P. Blood stem cells emerge from aortic endothelium by a novel type of cell transition. *Nature.* 2010;464(7285):112-115.

20. Espín-Palazón R, Stachura DL, Campbell CA, et al. Proinflammatory signaling regulates hematopoietic stem cell emergence. *Cell.* 2014;159(5): 1070-1085.

21. Li Y, Esain V, Teng L, et al. Inflammatory signaling regulates embryonic hematopoietic stem and progenitor cell production. *Genes Dev.* 2014; 28(23):2597-2612.

22. Sawamiphak S, Kontarakis Z, Stainier DY. Interferon gamma signaling positively regulates hematopoietic stem cell emergence. *Dev Cell.* 2014; 31(5):640-653.

23. Theodore LN, Hagedorn EJ, Cortes M, et al. Distinct Roles for Matrix Metalloproteinases 2 and 9 in Embryonic Hematopoietic Stem Cell Emergence, Migration, and Niche Colonization. *Stem Cell Reports.* 2017;8(5):1226-1241.

24. Travnickova J, Tran Chau V, Julien E, et al. Primitive macrophages control HSPC mobilization and definitive haematopoiesis. *Nat Commun.* 2015; 6(1):6227.

25. Mahony CB, Fish RJ, Pasche C, Bertrand JY. tfec controls the hematopoietic stem cell vascular niche during zebrafish embryogenesis. *Blood.* 2016;128(10):1336-1345.

26. Tamplin OJ, Durand EM, Carr LA, et al. Hematopoietic stem cell arrival triggers dynamic remodeling of the perivascular niche. *Cell.* 2015;160(1-2): 241-252.

27. Mahony CB, Pasche C, Bertrand JY. Oncostatin M and Kit-Ligand Control Hematopoietic Stem Cell Fate during Zebrafish Embryogenesis. *Stem Cell Reports.* 2018;10(6):1920-1934.

28. Bruno E, Luikart SD, Long MW, Hoffman R. Marrow-derived heparan sulfate proteoglycan mediates the adhesion of hematopoietic progenitor cells to cytokines. *Exp Hematol.* 1995;23(11):1212-1217.

29. Gupta P, Oegema TR Jr, Brazil JJ, Dudek AZ, Slungaard A, Verfaillie CM. Structurally specific heparan sulfates support primitive human hematopoiesis by formation of a multimolecular stem cell niche. *Blood.* 1998;92(12):4641-4651.

30. Roberts R, Gallagher J, Spooncer E, Allen TD, Bloomfield F, Dexter TM. Heparan sulphate bound growth factors: a mechanism for stromal cell mediated haemopoiesis. *Nature.* 1988;332(6162):376-378.

31. Gomez GA, Veldman MB, Zhao Y, Burgess S, Lin S. Discovery and characterization of novel vascular and hematopoietic genes downstream of etsrp in zebrafish. *PLoS One.* 2009;4(3):e4994.

32. Spicer AP, Joo A, Bowling RA Jr. A hyaluronan binding link protein gene family whose members are physically linked adjacent to chondroitin sulfate proteoglycan core protein genes: the missing links. *J Biol Chem.* 2003;278(23):21083-21091.

33. Day AJ, Prestwich GD. Hyaluronan-binding proteins: tying up the giant. *J Biol Chem.* 2002;277(7):4585-4588.

34. Watanabe H, Yamada Y. Mice lacking link protein develop dwarfism and craniofacial abnormalities. *Nat Genet.* 1999;21(2):225-229.

35. Long KR, Newland B, Florio M, et al. Extracellular Matrix Components HAPLN1, Lumican, and Collagen I Cause Hyaluronic Acid-Dependent Folding of the Developing Human Neocortex. *Neuron.* 2018;99(4):702-719.e6.

36. Kaur A, Ecker BL, Douglass SM, et al. Remodeling of the collagen matrix in aging skin promotes melanoma metastasis and affects immune cell motility. *Cancer Discov.* 2019;9(1):64-81.

37. Ecker BL, Kaur A, Douglass SM, et al. Age-Related Changes in HAPLN1 Increase Lymphatic Permeability and Affect Routes of Melanoma Metastasis. *Cancer Disc.* 2019;9(1):82-95.

38. Foscarin S, Ponchione D, Pajaj E, et al. Experience-dependent plasticity and modulation of growth regulatory molecules at central synapses. *PLoS One.* 2011;6(1):e16666.

39. Eskici NF, Erdem-Ozdamar S, Dayangac-Erden D. The altered expression of perineuronal net elements during neural differentiation. *Cell Mol Biol Lett.* 2018;23(1):5.

40. Gaál B, Kecskes S, Matesz C, Birinyi A, Hunyadi A, Rácz É. Molecular composition and expression pattern of the extracellular matrix in a mossy fiber-generating precerebellar nucleus of rat, the prepositus hypoglossi. *Neurosci Lett.* 2015;594:122-126.

41. Kecskes S, Gaál B, Rácz É, Birinyi A, Hunyadi A, Matesz C. Extracellular matrix molecules exhibit unique expression pattern in the climbing fiber-generating precerebellar nucleus, the inferior olive. *Neuroscience.* 2015;284:412-421.

42. Dick G, Tan CL, Alves JN, et al. Semaphorin 3A binds to the perineuronal nets via chondroitin sulfate type E motifs in rodent brains. *J Biol Chem.* 2013;288(38):27384-27395.

43. Beurdeley M, Spatazza J, Lee HH, et al. Otx2 binding to perineuronal nets persistently regulates plasticity in the mature visual cortex. *J Neurosci.* 2012;32(27):9429-9437.

44. Derrick CJ, Sánchez-Posada J, Hussein F, et al. Asymmetric Hapln1a drives regionalised cardiac ECM expansion and promotes heart morphogenesis in zebrafish development. *Cardiovasc Res.* 2021;cvab004.

45. Govindan J, Iovine MK. Hapln1a is required for connexin43-dependent growth and patterning in the regenerating fin skeleton. *PLoS One.* 2014; 9(2):e88574.

46. Govindan J, Tun KM, Iovine MK. Cx43-Dependent Skeletal Phenotypes Are Mediated by Interactions between the Hapln1a-ECM and Sema3d during Fin Regeneration. *PLoS One.* 2016;11(2):e0148202.

47. Westerfield M. The zebrafish book: A guide for the laboratory use of zebrafish (Brachydanio rerio) Eugene, OR: University of Oregon Press; 1994.

48. Zhu H, Traver D, Davidson AJ, et al. Regulation of the lmo2 promoter during hematopoietic and vascular development in zebrafish. *Dev Biol.* 2005; 281(2):256-269.

49. Traver D, Paw BH, Poss KD, Penberthy WT, Lin S, Zon LI. Transplantation and in vivo imaging of multilineage engraftment in zebrafish bloodless mutants. *Nat Immunol.* 2003;4(12):1238-1246.

50. Jin SW, Beis D, Mitchell T, Chen JN, Stainier DY. Cellular and molecular analyses of vascular tube and lumen formation in zebrafish. *Development.* 2005;132(23):5199-5209.

51. Chi NC, Shaw RM, De Val S, et al. Foxn4 directly regulates tbx2b expression and atrioventricular canal formation. *Genes Dev.* 2008;22(6): 734-739.

52. North TE, Goessling W, Walkley CR, et al. Prostaglandin E2 regulates vertebrate haematopoietic stem cell homeostasis. *Nature.* 2007;447(7147): 1007-1011.

53. Ganis JJ, Hsia N, Trompouki E, et al. Zebrafish globin switching occurs in two developmental stages and is controlled by the LCR. *Dev Biol.* 2012; 366(2):185-194.

54. Kirby BB, Takada N, Latimer AJ, et al. In vivo time-lapse imaging shows dynamic oligodendrocyte progenitor behavior during zebrafish development. *Nat Neurosci.* 2006;9(12):1506-1511.

55. Renshaw SA, Loynes CA, Trushell DM, Elworthy S, Ingham PW, Whyte MK. A transgenic zebrafish model of neutrophilic inflammation. *Blood.* 2006;108(13):3976-3978.

56. Ellett F, Pase L, Hayman JW, Andrianopoulos A, Lieschke GJ. mpeg1 promoter transgenes direct macrophage-lineage expression in zebrafish. *Blood.* 2011;117(4):e49-e56.

57. Thisse C, Thisse B, Schilling TF, Postlethwait JH. Structure of the zebrafish snail1 gene and its expression in wild-type, spadetail and no tail mutant embryos. *Development.* 1993;119(4):1203-1215.

58. Gao L, Li D, Ma K, et al. TopBP1 Governs Hematopoietic Stem/Progenitor Cells Survival in Zebrafish Definitive Hematopoiesis. *PLoS Genet.* 2015;11(7):e1005346.

59. Källberg M, Wang H, Wang S, et al. Template-based protein structure modeling using the RaptorX web server. *Nat Protoc.* 2012;7(8):1511-1522.

60. Kelley LA, Mezulis S, Yates CM, Wass MN, Sternberg MJ. The Phyre2 web portal for protein modeling, prediction and analysis. *Nat Protoc.* 2015; 10(6):845-858.

61. Yang J, Yan R, Roy A, Xu D, Poisson J, Zhang Y. The I-TASSER Suite: protein structure and function prediction. *Nat Methods.* 2015;12(1):7-8.

62. Tadros W, Lipshitz HD. The maternal-to-zygotic transition: a play in two acts. *Development.* 2009;136(18):3033-3042.

63. Kissa K, Murayama E, Zapata A, et al. Live imaging of emerging hematopoietic stem cells and early thymus colonization. *Blood.* 2008;111(3): 1147-1156.

64. Hultman KA, Bahary N, Zon LI, Johnson SL. Gene Duplication of the zebrafish kit ligand and partitioning of melanocyte development functions to kit ligand a. *PLoS Genet.* 2007;3(1):e17.

65. Yuzawa S, Opatowsky Y, Zhang Z, Mandiyan V, Lax I, Schlessinger J. Structural basis for activation of the receptor tyrosine kinase KIT by stem cell factor. *Cell.* 2007;130(2):323-334.

66. Zhang Z, Zhang R, Joachimiak A, Schlessinger J, Kong XP. Crystal structure of human stem cell factor: implication for stem cell factor receptor dimerization and activation. *Proc Natl Acad Sci USA.* 2000;97(14):7732-7737.

67. Elegheert J, Bracke N, Pouliot P, et al. Allosteric competitive inactivation of hematopoietic CSF-1 signaling by the viral decoy receptor BARF1. *Nat Struct Mol Biol.* 2012;19(9):938-947.

68. Savvides SN, Boone T, Andrew Karplus P. Flt3 ligand structure and unexpected commonalities of helical bundles and cystine knots. *Nat Struct Biol.* 2000;7(6):486-491.

69. Verstraete K, Vandriessche G, Januar M, et al. Structural insights into the extracellular assembly of the hematopoietic Flt3 signaling complex. *Blood.* 2011;118(1):60-68.

70. Guo J, Jie W, Shen Z, et al. SCF increases cardiac stem cell migration through PI3K/AKT and MMP-2/-9 signaling. *Int J Mol Med.* 2014;34(1): 112-118.

71. Nandadasa S, O'Donnell A, Murao A, et al. (2020). The versican-hyaluronan complex provides an essential extracellular matrix niche for Flk1+ hematoendothelial progenitors. *bioRxiv*, 753418.

72. Azzoni E, Frontera V, McGrath KE, et al. Kit ligand has a critical role in mouse yolk sac and aorta-gonad-mesonephros hematopoiesis. *EMBO Rep.* 2018;19(10):19.

73. Batsivari A, Rybtsov S, Souilhol C, et al. Understanding Hematopoietic Stem Cell Development through Functional Correlation of Their Proliferative Status with the Intra-aortic Cluster Architecture. *Stem Cell Reports.* 2017;8(6):1549-1562.

74. Rybtsov S, Batsivari A, Bilotkach K, et al. Tracing the origin of the HSC hierarchy reveals an SCF-dependent, IL-3-independent CD43(−) embryonic precursor. *Stem Cell Reports.* 2014;3(3):489-501.

75. Lancino M, Majello S, Herbert S, et al. Anisotropic organization of circumferential actomyosin characterizes hematopoietic stem cells emergence in the zebrafish. *eLife.* 2018;7:7.

76. Poullet N, Golushko I, Lorman V, et al. Mechanical instabilities of aorta drive blood stem cell production: a live study. *Cell Mol Life Sci.* 2020; 77(17):3453-3464.